Superbright Multifluorescent Core–Shell Mesoporous Nanospheres as Trackable Transport Carrier for Drug

Juying Lei, Lingzhi Wang,* and Jinlong Zhang*

Key Lab for Advanced Materials and Institute of Fine Chemicals, East China University of Science and Technology, 130 Meilong Road, Shanghai, 200237, People's Republic of China

ABSTRACT A novel kind of monodisperse core–shell silica nanosphere composed of a fluorescent solid core and a mesoporous shell has been successfully fabricated. These nanospheres exhibit multifluorescent signals under a single-wavelength excitation as a result of the solid silica core that is doped with three kinds of dyes and that can produce effective fluorescence resonance energy transfer. The fluorescent signal of a single nanosphere is about 700 times brighter than its constituent fluorophores. X-ray diffraction, transmission electron microscopy, and N_2 adsorption–desorption isotherms reveal that these nanospheres possess abundant mesopores in the shell. Combining the advantages of extremely bright multifluorescent signals excited with a single wavelength and an abundant mesoporous system, this core–shell silica nanosphere is designed for the simultaneous monitoring of fluorescence of *in vivo* multiple-target drug transport. Experiments on drug loading and release in addition to studies on cell uptake reveal that these nanospheres not only show good drug storage and sustained release capacity but also demonstrate biocompatibility and mutlifluorescent labeling capacity for biological systems.

KEYWORDS: core–shell nanoparticles · multifluorescence · mesoporous silica · transport carrier

Mesoporous silica materials that are nontoxic in nature and have tunable pore diameter with high specific surface area and abundant Si–OH groups on the pore surface are promising candidates as drug-transport carriers in living systems.[1–10] However, drug-transport carriers entering into biological host systems may not be able to effectively locate the target organs due to the complicated *in vivo* environment, a challenge that makes the monitoring of the transport routes for drug-transport carriers important, especially for those carrying toxic anticancer drugs. Fluorescent labeling is a real-time, simple, and effective way to monitor the route of drug-transport carriers in a living system. Mesoporous structures doped with dye molecules have been demostrated to show novel and different fluorescent behavior compared with dye molecules in solution.[11–17] Recently, nanocomposites combining mesoporous structures with fluorescent molecules have attracted considerable attention for application as drug-transport carriers. Several research groups have made considerable progress in this field. For example, Yang *et al*. functionalized MCM-41 with luminescent YVO_4:Eu^{3+} *via* a Pechini sol–gel process.[18] The obtained YVO_4:Eu^{3+} and MCM-41 composite maintained the mesoporous structure of MCM-41 and the red luminescence property of YVO_4:Eu^{3+}, which has great potential for drug transport and disease therapy, as a consequence of the fact that it can be easily identified and tracked. Lin *et al*. reported mesoporous silica nanoparticles end-capped with CdS nanoparticles, which endowed the system with fluorescence that can be used to observe the transport and release of drug molecules.[19] Zink *et al*. functionalized fluorescent dye molecules onto mesoporous silica nanoparticles using a co-condensation method.[20] This modification of the particles involves incorporating fluorescein along the pore walls, enabling the cellular uptake of the nanoparticles to be monitored by fluorescence microscopy. However, more research is still required to synthesize monodisperse, biocompatible, and photostable fluorescent mesoporous silica nanoparticles with unimpeded access and high loading capacity for application as trackable drug-transport carrier systems.

Moreover, with the growing diversification and complication of diseases, a demand thus arises for multiple-target drug transport independent of whether the drug is taken up by a living body through the same or different administration routes. Along with this demand, the simultaneous

* Address correspondence to jlzhang@ecust.edu.cn, wlz@ecust.edu.cn.

Received for review August 11, 2010 and accepted March 29, 2011.

Published online March 29, 2011
10.1021/nn103254g

tracking and monitoring of multiple-target transfer routes of carriers loaded with different drugs becomes more and more important to ensure their precise location, which requires a combination of a barcode library and excellent drug-transport carriers. Fluorescent resonance energy transfer (FRET) pairs can engender abundant fluorescent signals excited with a single wavelength. Therefore, to find a convenient way to realize the combination of FRET and mesoporous silica materials will be of great interest and potential.

Recently, our group reported the novel fluorescence performance of duel-dye-doped FRET mesoporous silica nanoparticles, which are fabricated by doping and fixing one or two kinds of oligosilicate fluorescent dots encapsulated with dye molecules into the pore channels of mesoporous silica nanoparticles.[21] This system can engender two fluorescent signals under a single-wavelength excitation. However, for the application as the transport carrier for drugs, the oligosilicate fluorescent dots in the pore channels may make the drug molecules inaccessible to the mesopores or have detrimental effects on the drug molecules.

In this paper, to the best of our knowledge we report for the first time a monodisperse multicolor core–shell nanocomposite, using a triple-dye-doped FRET silica nanoparticle as the core and mesoporous silica as the shell. To simultaneously achieve multifluorescence and high-capacity drug loading, the dye molecules are encapsulated into the nonporous silica core, not the mesoporous channels of the silica shell. This kind of core–shell structure not only presents open and unimpeded mesoporous channels but also exhibits multiple and extremely bright fluorescence signals under a single-wavelength excitation, which provides a suitable nanoplatform for the fluorescence-monitored *in vivo* drug transport with different transport routes to address the growing need for sensitive monitoring of multiple-target drug-transport routes. The unique and excellent fluorescent performance of this core–shell composite loaded with drug molecules was specifically studied by confocal fluorescence images. Moreover, the biocompatibility and fluorescent performance of this composite in the biological system were also studied.

RESULTS AND DISCUSSION

Preparation of Mesoporous Nanospheres (MNSs). The preparation of MNSs takes three steps: (1) the premodification of the dye molecules: 3-aminopropyltriethoxysilane (APTS) reacts with fluorescein isothiocyanate (FITC), rhodamine B isothiocyanate (RBITC), and rhodamine 101 succinimide (R101-SE) to form three types of dye–APTS conjugates; (2) the hydrolysis and co-condensing of dye–APTS and tetraethylorthosilicate (TEOS) to produce dye-doped silica cores (DSCs); (3) fabricating a mesoporous layer on the DSCs to form

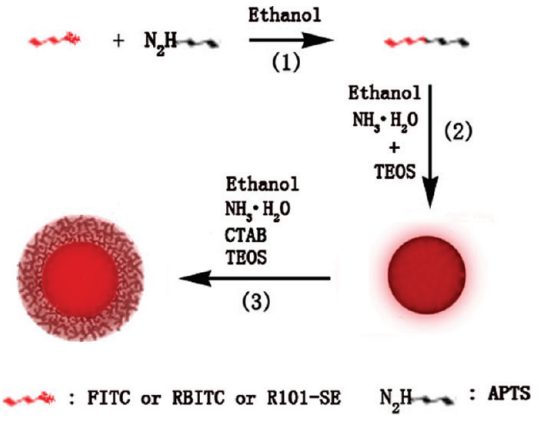

Scheme 1. Synthetic route for multifluorescent core–shell MNSs.

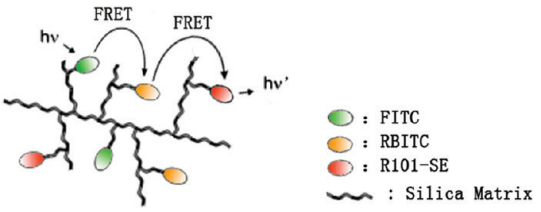

Scheme 2. Representation of the FRET processes in the MNSs.

core–shell MNSs by adopting the modified Stöber method (Scheme 1).

In the first step, using a method reported by Wiesner's group,[22–28] amine-reactive dye molecules FITC, RBITC, and R101-SE were covalently linked to the silane coupling agent APTS; in this way dye molecules are less prone to leak out from the silica matrix than fluorophores incorporated into the silica particles by other methods.[29] To obtain multiple fluorescent signals with different colors and intensities, the three types of dye–APTS conjugates were simultaneously introduced into the silica cores with various ratios. The three tandem dyes were carefully chosen to allow for efficient fluorescence resonance energy transfer because of their effective spectral overlapping (Figure 3a). In the triple-dye-doped silica cores, FITC can be used as the common donor for RBITC and R101-SE, while RBITC acts as an acceptor for FITC and a donor for R101-SE, which can lead to effective fluorescence energy transfer under a single-wavelength excitation (Scheme 2).

Mesostructure of MNSs. The initial dye-doped silica cores are uniform with an average diameter of 80.4 nm determined by manually measuring over 100 particles from TEM (Figure 1a), where the standard deviation is 4.86 nm. These uniform cores result in a narrow distribution of the final particle sizes since the TEM images of MNSs (Figure 1b and c) show that the mesoporous silica coating is also uniform. The average diameter of the core–shell nanoparticles is 138.6 nm with a standard deviation of 4.3 nm. After removing cetyltrimethyl ammonium bromide (CTAB), which

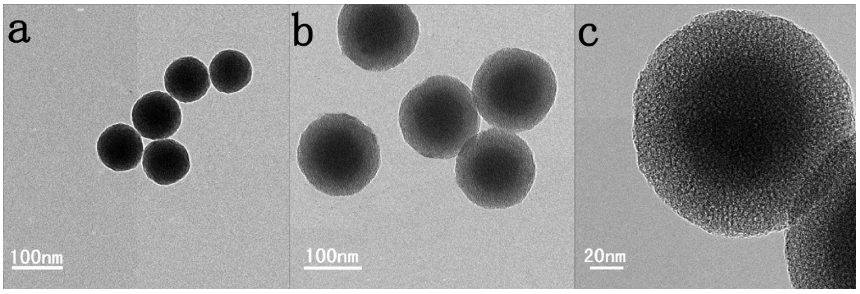

Figure 1. TEM images of DSCs (a) and MNSs (b and c).

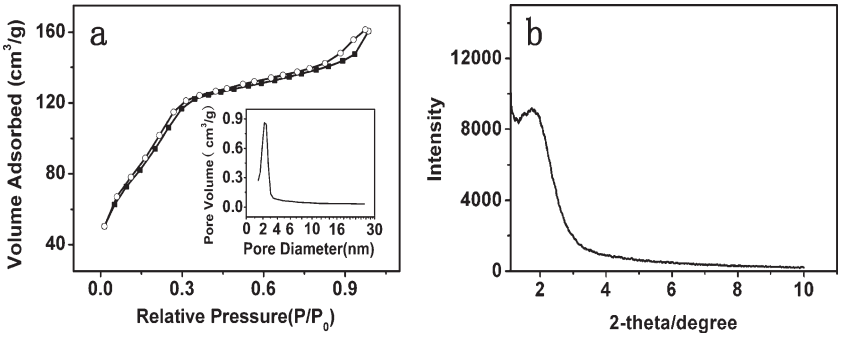

Figure 2. (a) Nitrogen adsorption/desorption isotherms and pore size distributions (inset); (b) low-angle XRD pattern of MNSs.

serves as the porogen during the growth process of the mesoporous layer, the pores are revealed to be diverging from the center to the fringes (Figure 1c).

The N_2 adsorption/desorption isotherms (Figure 2a) exhibit a typical type IV isotherm of mesoporous material. The pore size calculated using the BJH method (Figure 2a (inset)) is about 2.4 nm. The BET surface area and the BJH desorption cumulative volume of pores of MNSs are 378 $m^2\ g^{-1}$ and 0.249 $cm^3\ g^{-1}$, respectively, which are considerably large since all the solid cores have been included in the calculations. The XRD pattern shown in Figure 2b exhibits a broad peak in the low-angle region at approximately $2\theta = 2°$ and no observable fine peak, which is typical for poorly ordered hexagonal symmetry or amorphous wormlike mesoporous channels. The spherical shape of mesoporous particles can be ascribed to the distortion from hexagonal symmetry, and the peak in the low-angle region can be indexed to (100) diffraction.[30]

Fluorescence of MNSs. The average amount of dye molecules encapsulated in each nanosphere was calculated in order to compare the brightness of a single nanosphere with a single dye molecule. We employed FITC-MNSs doped only with FITC as a control study because of the difficulty of characterizing triple-dye-doped MNSs, where the fluorescence intensity corresponding to FITC, RBITC, or R101-SE is influenced by energy transfer. The dye molecule numbers for each particle was calculated as follows: First, the standard curve of absorbance versus concentration for FITC was plotted. Then the loading amount of FITC molecules per gram of silica core was calculated to be about 67.6% from the maximum absorption intensity of the filtrated FITC solution. Subsequently, the number of nanoparticles per gram was determined by drying and weighing a certain volume of nanoparticle solution. The number of dye molecules per nanoparticle was finally calculated to be about 900 based on the above experiment. To compare the fluorescence intensities of a single FITC dye molecule and a single FITC-doped MNSs, the titration curves of the fluorescence intensity as a function of the FITC dye concentration and FITC-doped MNSs concentration were plotted, respectively. The intensity and the concentration were linearly dependent for the extremely dilute solution, and the fluorescence intensities of the single FITC molecule and FITC-doped MNSs were approximately obtained by directly reading the axis intercept of intensity. The single FITC-doped MNS was calculated to be 700 times brighter than the corresponding single FITC molecule. The above results indicate MNSs prepared by the method shown in Scheme 1 exhibit extraordinarily strong fluorescence, although partial fluorescence quenching occurred according to the dye molecule numbers and fluorescence intensity per particle. Actually, on the basis of the calculated local molar concentration of FITC in the solid core (5.6×10^{-3} M), the fluorescence quenching is considerably reduced since FITC dispersed in homogeneous solution with the same concentration suffers severe self-quenching due to intermolecular collisions. Different from the homogeneous solution, the dye molecules

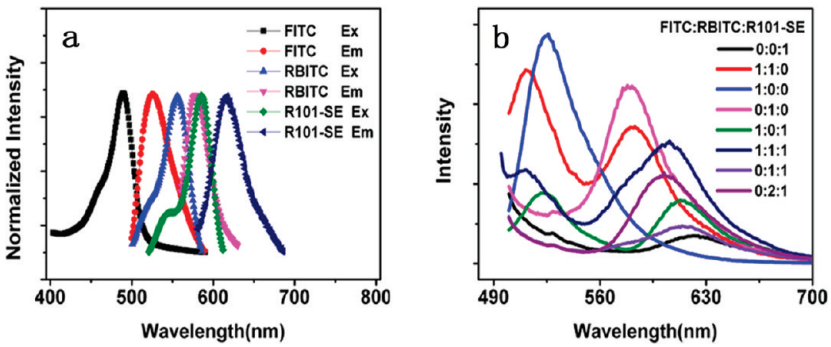

Figure 3. (a) Excitation and emission spectra of FITC, RBITC, and R101-SE dyes; (b) fluorescence spectra of MNSs co-doped with FITC, RBITC, and R101-SE with different doping ratios excited at 488 nm.

encapsulated in the solid matrix are not free; that is, they are restricted to a fixed area. Therefore, the quenching caused by intermolecular collision can be well reduced. It is possible that the fluorescence quenching arising from the interaction between dye molecules in the solid core may be completely avoided by decreasing the loading amount of dye molecules. We studied the relation between fluorescence intensity and dye loading amount and found that the fluorescence intensity actually improves with an appropriate decrease in the amount of dye molecules. However, the improved dispersive state of dye molecules is disadvantageous to the FRET process since it leads to the improved distance between different dye molecules. A little excessive doping amount of dye molecule can ensure that adequate dye molecules can be involved in the FRET process. In fact, compared with the fluorescence intensity of mesoporous silica by introducing dye molecules in the pore channels, which is only 50 times brighter than the corresponding single dye molecule,[21] the fluorescence intensity of the current core–shell MNSs is much stronger. The improved fluorescence intensity of the core–shell MNSs is attributed to the more effective shielding of dye molecules in the solid core than in the open pore channel from the outer environment, which is advantageous to the application of *in vivo* fluorescence monitoring.

To form colorfully fluorescent MNSs, the dye molecules FITC, RBITC, and R101-SE were selected in our model because of their effective spectral overlapping, as shown in Figure 3a, which permits the energy transfer among the three tandem dyes and can form various fluorescent signals by using a single excitation wavelength. The fluorescence spectra of the MNSs doped with FITC, RBITC, and R101-SE are shown in Figure 3b. The simultaneous appearance of the emissions of three dyes excited at 488 nm is obviously observed, which demonstrates efficient FRET between the above three dye molecules. The fluorescence emission shape varies with the doping ratio, indicating a finely controllable fluorescent signal is easily achieved. The covalent trichromophoric doping method presented here can be further extended to more than three chromophores, and the FRET MNSs strategy can be applied to any energy transfer dye series for the generation of more colorful fluorescence signals.

To acquire more information about the FRET in the core–shell nanospheres, calculations of the average donor–acceptor distance between two FRET dye molecules as well as the energy transfer efficiency were carried out. The energy transfer efficiency, denoted as E, was calculated by comparing the fluorescence intensity of the donor alone (F_D) and in the presence of the acceptor (F_{DA}) according to eq 1,[31–33] where R_o is the Förster radius and R is the average donor–acceptor distance.

$$E = \frac{{R_o}^6}{R^6 + {R_o}^6} = 1 - \frac{F_{DA}}{F_D} \quad (1)$$

Using single FITC-doped nanospheres and FITC–RBITC (1:1) co-doped nanospheres, we calculated a transfer efficiency of 15.76% based on the fluorescence intensity of both the nanospheres. This transfer efficiency values then was used to calculate R according to eq 2, a rearrangement of eq 1, along with eq 3 and eq 4:[34]

$$R = R_o[(1 - E) - 1]^{1/6} \quad (2)$$

$${R_o}^6 = \frac{9000(\ln 10)\kappa^2\phi_D}{128\pi^5\eta^4 N}J(\lambda) \quad (3)$$

$$J(\lambda) = \int F_D(\lambda)\,\varepsilon_A(\lambda)\lambda^4\,d\lambda \quad (4)$$

In eq 3, η is the refractive index of the aqueous medium (1.33), κ^2 is the orientation factor resulting from the vector nature of dipole transitions, generally assumed to be 2/3, N is Avogadro's number, φ_D is the donor quantum yield, $F_D(\lambda)$ is donor (FITC) emission (normalized to unity) as a function of wavelength λ, and ε_A is the extinction coefficient of the acceptor (RBITC). The term R_o has the units of distance and is unique for each donor–acceptor pair. The above Förster model has been employed to calculate the average distances between the donor–acceptor pair.[35–39]

The UV–vis absorption spectrum of an aqueous RBITC solution of known concentration and the

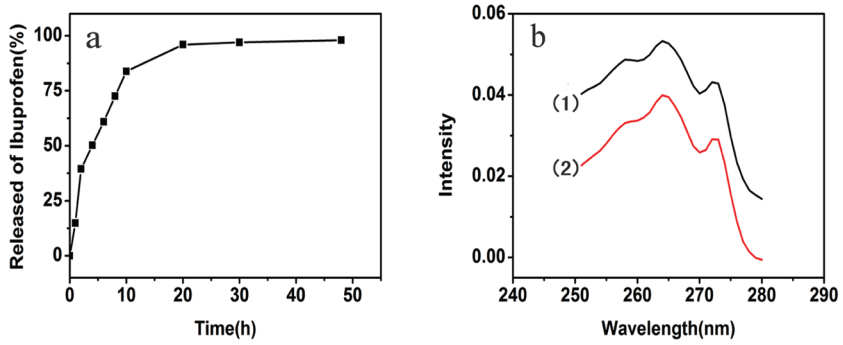

Figure 4. (a) Release of IBU from MNSs; (b) UV−vis spectra of IBU in simulated body fluid solution (1) and the release media after IBU is released from the MNSs−IBU system (2).

Figure 5. Confocal fluorescence image of a mixture of eight types of MNSs−IBU under 488 nm argon-ion laser excitation.

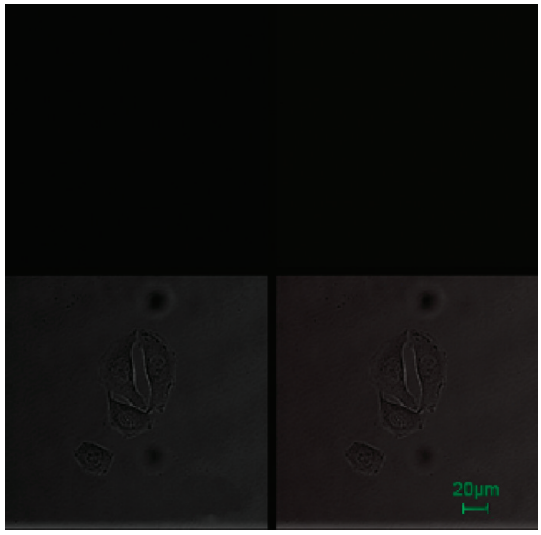

Figure 6. Fluorescence confocal micrograph of HeLa cells without MNSs. Upper: fluorescence image. Lower left: differential interference contrast (DIC) image. Lower right: merged image.

emission spectrum of FITC (Figure 3) are used to calculate the spectral overlap integral in the rate expression. The resulting calculated spectral overlap using eq 4 is 2×10^{18}. The quantum yield, φ, of the FITC donor in the core−shell nanospheres was estimated to be 0.75 by using the relationship $\varphi = \tau/\tau_i$,[37,40] where τ_i is the intrinsic lifetime of the FITC excited state. Using the previously reported value of $\tau_i = 4.5$ ns[34] and an average lifetime of 3.3 ns measured for FITC in core−shell nanospheres, a value of $\varphi_D = 0.73$ is calculated. Inserting the above values into eq 3 gives the Förster radius of 1.13 nm. Consequently, the average donor−acceptor distance, R, was calculated to be 2.48 nm. It is known that when the donor and the acceptor are in close proximity (2−8 nm), the excited-state energy from the donor can be transferred to the acceptor *via* dipole−dipole coupling between the chromophores.[42] Therefore, the 2.48 nm separation distance offers the optimal space for the occurrence of FRET within the core−shell nanospheres, leading to abundant fluorescent signals under a single-wavelength excitation.

Moreover, to check if there was any dye leaking from MNSs, the FITC-MNSs were dissolved in 0.1 M phosphate buffer (pH = 7.4), which was followed by ultrasound and centrifugation treatment. The fluorescence intensity of the supernatant was close to that of the background signal. The above experiment was repeated three times, which obviously indicates that dye molecules covalently bound to the silica matrix are very stable and do not readily leach from the solid core. Moreover, there was no noticeable change in the fluorescence intensity of the FITC-MNSs after successive illumination experiments over 2 h in duration with a UV source (300 W mercury lamp). This result indicates dye molecules doped into the silica core are not prone to photobleaching. This is because the solid and porous silica framework protect the fluorescent dye from the environment, which suggests that these superbright and multifluorescent core−shell nanocomposites can be applied and maintained in complex *in vivo* environments and be monitored.

Drug Loading and Release. To investigate the drug loading and release performance of MNSs, we selected ibuprofen (IBU) as a model drug, which has been extensively investigated for sustained and controlled drug release due to its short biological half-life (2 h), good pharmacological activity, and suitable molecule

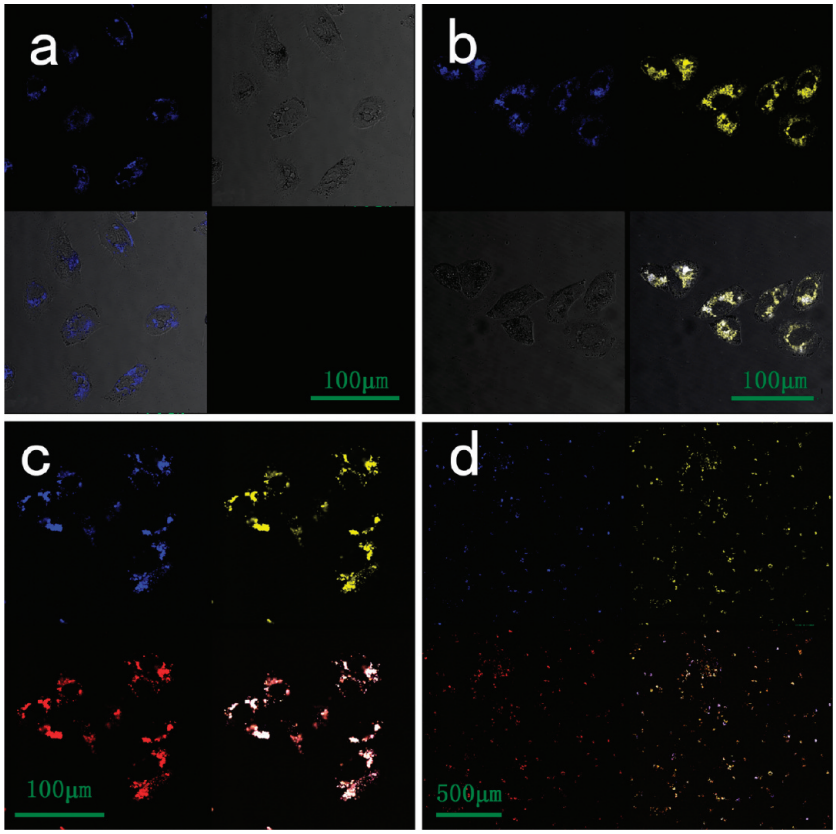

Figure 7. Fluorescence confocal micrographs of HeLa cells after 10 h incubation with different MNSs: (a) FITC-doped MNSs. Upper left: fluorescence image. Upper right: differential interference contrast (DIC) image. Lower left: merged image. (b) FITC and RBITC co-doped MNSs. Upper left: fluorescence image of FITC channel. Upper right: fluorescence image of RBITC channel. Lower left: DIC image. Lower right: merged image of FITC channel, RBITC channel, and DIC. (c) FITC, RBITC, and R101-SE co-doped MNSs. Upper left: fluorescence image of FITC channel. Upper right: fluorescence image of RBITC channel. Lower left: fluorescence image of R101-SE channel. Lower right: merged image of FITC, RBITC, and R101-SE channel. (d) Mixture of cells incubated with MNSs co-doped with FITC, RBITC, and R101-SE with different ratios. All these images were acquired under 488 nm argon-ion laser excitation. The emissions of FITC, RBITC, and R101-SE are colored blue, yellow, and red.

size.[10] The drug was dissolved in hexane (1 mg mL^{-1}), and then the MNS sample was added. The mixture was stirred for 24 h while making sure the evaporation of hexane was prevented. The amount of IBU loaded in the MNSs was determined by UV spectrometry, reading at 264 nm, resulting in about 12 wt % with respect to the starting addition.

IBU molecules were released from samples *via* a diffusion-controlled mechanism. Figure 4a shows the IBU release behaviors from the MNSs–IBU system over a 48 h period in simulated body fluid. It can be seen that burst releases are obtained within 2 h from the MNSs–IBU system, and then a steady release follows; 95% of the adsorbed IBU is released from MNSs within 48 h. It is obvious that this MNSs–IBU system has sustained release behavior.

In addition, Figure 4b shows the UV absorbance spectra of the release media after IBU is released from the MNSs–IBU system. It can be seen that the positions of the absorbance peaks remain unchanged and no new band appears. Therefore, the IBU drug stored in MNSs is released in its original form and no impurity especially for the dye molecule is released. The morphology of the nanoparticles and structure of the mesopores remained unchanged after immersing into a simulated body fluid, as shown in the Supporting Information.

To demonstrate the coding and labeling performances of the MNSs, confocal fluorescent images of MNSs–IBU were recorded (Figure 5). Eight kinds of MNSs–IBU doped with FITC, RBITC, and R101-SE with different ratios were mixed together and excited with a 488 nm argon-ion laser, and distinguishable bright colors were clearly and simultaneously observed. This model demonstrated the potential of these multicolor MNSs for application as a fluorescently trackable carrier, which can be loaded with different drugs and simultaneously monitored.

Cell Uptake. Human cervical cancer (HeLa) cells were employed to investigate the fluorescence performance and biocompatibility of MNSs in biological systems. The cancer cells were incubated with MNSs of different colors in the growth medium with serum, penicillin, and streptomycin for 10 h and analyzed by confocal microscopy. Figure 6 shows that the cells without MNSs obviously have no fluorescence under

argon-ion laser excitation. Figure 7 clearly shows that MNSs can actually enter into the cell cytoplasm and form strong fluorescent signals under 488 nm argon-ion laser excitation. The fluorescence color of MNSs varies with the doping ratio of FITC, RBITC, and R101-SE. The confocal microscopy images reveal that the cells incubated with different MNSs can exhibit multiple emission colors under a single-wavelength argon-ion laser excitation. The cells incubated with single FITC-doped MNSs have only blue emission of FITC (Figure 7a), while cells with FITC and RBITC co-doped MNSs show two emissions simultaneously (upper left and upper right, Figure 7b) merged as bright yellow (lower right, Figure 7b) and cells with FITC, RBITC, and R101-SE co-doped MNSs have three emissions (blue, yellow, and red) merged as pink-purple (lower right, Figure 7c). When cells are incubated with different kinds of MNSs mixed together, colorful signals are obtained (lower right, Figure 7d). The above results suggest that the core–shell MNSs are able to enter cells efficiently without any uptake-enhancing techniques and engender abundant fluorescent signals under a single-wavelength excitation, which can be ascribed to the efficient energy transfer within the core–shell nanospheres. The above results further corroborate that the multifluorescent nanospheres possess great potential application for the simultaneous labeling and monitoring of multiple-target drug transport.

CONCLUSION

In conclusion, we have successfully prepared a novel kind of fluorescent core–shell mesoporous nanosphere by combining triple-FRET and mesoporous characteristics. The significance of this study lies in the fact that we prepared superbright and multifluorescent core–shell MNSs, which may be loaded with different drugs and tracked simultaneously in living systems. We expect this study to open up a new perspective in the design of more multifunctional structures for trackable drug transport based on core–shell mesoporous silica nanospheres.

MATERIALS AND METHODS

Materials. FITC and RBITC were acquired from Amresco. *N*-Hydroxysuccinimide and *N*,*N*′-dicyclohexyl carbodiimide were supplied by Shanghai Kayon Biological Technology Co., Ltd. R101 was purchased from Exiton Inc. IBU was obtained from Alfa Aesor. CTAB, absolute ethanol, TEOS, and ammonium hydroxide were purchased from Shanghai Sinopharm Chemical Reagent Co., Ltd., China. APTS was supplied by Shanghai Yaohua Chemical Plant. Distilled deionized water was used for the preparation of all aqueous solutions. All starting materials and solvents were used as received without further purification.

Synthesis of R101-SE. R101 (591 mg, 1 mmol) and *N*-hydroxysuccinimide (115 mg, 1 mmol) were dissolved in dichloromethane (40 mL). Then *N*,*N*′-dicyclohexyl carbodiimide (206 mg, 1 mmol) was added. The mixture was stirred at 318 K for 48 h followed by cooling and filtering. The organic filtrate was evaporated, and the residue was purified by chromatography over silica (eluent, CH_2Cl_2–MeOH, 100:1) to afford R101-SE.

^{1}H NMR (400 MHz, $CDCl_3$, δ): 8.414 (d, J = 8.0 Hz, 1H, ArH), 7.935 (t, J = 7.6 Hz, 1H, ArH), 7.797 (t, J = 7.8 Hz, 1H, ArH), 7.416 (d, J = 7.6 Hz, 1H, ArH), 6.589 (s, 2H, ArH), 3.559–3.484 (m, 8H, CH_2), 3.077–2.984 (m, 4H, CH_2), 2.772–2.640 (m, 8H, CH_2), 2.138–1.054 (m, 8H, CH_2). ^{13}C NMR (100 MHz, $CDCl_3$, δ): 168.957, 160.756, 152.640, 151.996, 151.258, 135.462, 134.790, 131.525, 131.392, 130.303, 125.587, 124.152, 112.592, 105.380, 50.937, 50.456, 27.583, 25.611, 20.554, 19.892, 19.651. MS (ESI+, *m*/*z*): $[M + H]^+$ calcd for $C_{37}H_{35}N_2O_5^+$, 588.26; found, 589.3. UV (H_2O): λ_{max} = 585 nm.

Synthesis of Dye–APTS Conjugates. For the synthesis of FITC–APTS and RBITC–APTS conjugates, FITC and RBITC were covalently attached to the APTS silane compound by a stable thiourea linkage, while R101-SE–APTS was attached by a steady amide linkage. Briefly, APTS (1.32 mL) and dye molecules (2.7 μmol) were combined in absolute ethanol (2 mL) under a dry nitrogen atmosphere and stirred magnetically overnight. The dye–APTS conjugate solution was protected from light during both the reaction and storage to prevent photobleaching. The conjugate was later used as the fluorescent silane reagent.

Synthesis of DSCs. The three dye–APTS conjugates were mixed at desired ratios and added to a clean glass reaction vessel containing pure ethanol (33.5 mL) and ammonium hydroxide (3.34 mL). The mixture was stirred for 24 h. TEOS (1.42 mL) was added afterward and stirred for another 24 h. After the reaction, the product mixture was centrifuged to collect the silica nanoparticles. The nanoparticles were further washed with ethanol and deionized water using centrifugation and decantation several times to remove the unreacted chemicals.

Synthesis of MNSs. To coat DSCs with a layer of mesoporous silica, DSCs (100 mg) were added to ethanol (190 mL) in a 500 mL reaction flask equipped with a stir bar. After 20 min of ultrasonic treatment, ammonium hydroxide (24 mL) and CTAB (1.0 g) were added to the mixture. The mixed solution was homogenized for 0.5 h to form a uniform dispersion. Then TEOS (250 μL) was added and the solution was stirred for 16 h. The obtained product was centrifuged and redispersed in ethanol. This purification process was repeated several times.

Finally, the CTAB templating agents were removed using an acid extraction process: The synthesized core–shell nanoparticles (100 mg) were suspended in EtOH (100 mL), and concentrated HCl (2 M, 5 mL) was added. The suspension was vigorously stirred for 24 h, and the materials were then collected *via* vacuum filtration, washed extensively with EtOH and distilled water, and dried under vacuum.

Dye Leaking Experiment. After the removal of surfactants (as mentioned above), MNSs were checked for any dye leakage. An aqueous suspension of MNSs (10 mg mL^{-1}) was first treated with ultrasound for 5 min and then centrifuged at 12 000 rpm for 15 min. The fluorescence of the supernatant was measured, and this experiment was repeated three times.

Drug Storage and Release. The IBU drug storage experiment was conducted as follows: MNSs (50 mg) were added into IBU hexane solution (10 mL) with a concentration of 1 mg mL^{-1} at room temperature. The vials were sealed to prevent the evaporation of hexane; then the mixture was stirred for 24 h. The IBU-loaded MNSs (MNSs–IBU) were separated from this solution by centrifugation and dried under vacuum at 333 K. The filtrates were vaporized and then dissolved in simulated body fluid of pH 7.4 (250 mL) and analyzed by UV/vis spectroscopy at a wavelength of 264 nm. The calibration curve of IBU was determined by taking absorbance measurements of IBU solutions at various concentrations.

A typical *in vitro* drug release experiment was performed as follows: the above MNSs−IBU materials were redispersed into simulated body fluid of pH 7.4 (10 mL) under stirring at a rate of 100 rpm. The release medium was removed for analysis every other hour by centrifuging at 12 000 rpm for 20 min. The solid residue was added to the same volume of fresh simulated fluid. The filtrates were analyzed with UV/vis spectroscopy at a wavelength of 264 nm, and the percentage of released drug molecules in the solution phase was calculated.

Uptake of MNSs into HeLa cells. HeLa cell lines were obtained from Cell Bank of Type Culture Collection of Chinese Academy of Sciences (Shanghai, China) and maintained using Rosewell Park Memorial Institute 1640 medium supplemented with 10% heat-inactivated bovine serum, penicillin (100 U mL^{-1}), and streptomycin (100 U mL^{-1}). HeLa cells were seeded into 35 mm glass-bottomed dishes coated with polylysine for 24 h prior to the experiment. After 24 h, the dishes were seeded with MNSs (0.2 mg mL^{-1}) in growth medium. After 10 h, the medium was removed and the cells were washed three times with phosphate-buffered saline. Images were acquired with a Leica TCS SP5 confocal unit.

Acknowledgment. This work was supported by National Nature Science Foundation of China (21007016), the Research Fund for the Doctoral Program of Higher Education (20070-251006), Science and Technology Commission of Shanghai Municipality (10520709900), and the Fundamental Research Funds for the Central Universities.

Supporting Information Available: Structure of the core−shell mesoporous silica nanoparticles after immersion into simulated body fluid and characterization details of R101-SE. This material is available free of charge *via* the Internet at http://pubs.acs.org.

REFERENCES AND NOTES

1. Lee, C. H.; Lo, L. W.; Mou, C. Y.; Yang, C. S. Synthesis and Characterization of Positive-Charge Functionalized Mesoporous Silica Nanoparticles for Oral Drug Delivery of an Anti-Inflammatory Drug. *Adv. Funct. Mater.* **2008,** *18*, 3283–3292.
2. Meng, H.; Liong, M.; Xia, T.; Li, Z.; Ji, Z.; Zink, J. I.; Nel, A. E. Engineered Design of Mesoporous Silica Nanoparticles to Deliver Doxorubicin and P-Glycoprotein siRNA to Overcome Drug Resistance in a Cancer Cell Line. *ACS Nano* 2010, in press. DOI: 10.1021/nn100690m.
3. Wang, L. S.; Wu, C. L.; Lu, S. Y.; Chang, L. L.; Teng, I. T.; Yang, C. M.; Ho, J. A. Biofunctionalized Phospholipid-Capped Mesoporous Silica Nanoshuttles for Targeted Drug Delivery: Improved Water Suspensibility and Decreased Nonspecific Protein Binding. *ACS Nano* 2010, *4*, 4371−4379.
4. Muñoz, B.; Rámila, A.; Pérez-Pariente, J.; Díaz, I.; Vallet-Regí, M. MCM-41 Organic Modification as Drug Delivery Rate Regulator. *Chem. Mater.* **2003,** *15*, 500–503.
5. Mal, N. K.; Fujiwara, M.; Tanaka, Y. Photocontrolled Reversible Release of Guest Molecules from Coumarin-Modified Mesoporous Silica. *Nature* **2003,** *421*, 350–353.
6. Rosenholm, J. M.; Peuhu, E.; Eriksson, J. E.; Sahlgren, C.; Lindén, M. Targeted Intracellular Delivery of Hydrophobic Agents Using Mesoporous Hybrid Silica Nanoparticles as Carrier Systems. *Nano Lett.* **2009,** *9*, 3308–3301.
7. Rámila, A.; Muñoz, B.; Pérez-Pariente, J.; Vallet-Regí, M. Mesoporous MCM-41 as Drug Host System. *J. Sol-Gel Sci. Technol.* **2003,** *26*, 1199–1202.
8. Arcos, D.; López-Noriega, A.; Ruiz-Hernández, E.; Terasaki, O.; Vallet-Regí, M. Ordered Mesoporous Microspheres for Bone Grafting and Drug Delivery. *Chem. Mater.* **2009,** *21*, 1000–1009.
9. Doadrio, A. L.; Sousa, E. M.B.; Doadrio, J. C.; Pérez-Pariente, J.; Izquierdo-Barba, I.; Vallet-Regí, M. Mesoporous SBA-15 HPLC Evaluation for Controlled Gentamicin Drug Delivery. *J. Controlled Release* **2004,** *97*, 125–132.
10. Vallet-Regí, M.; Rámila, Real, A.; R, P. del.; Pérez-Pariente, J. A New Property of MCM-41: Drug Delivery System. *Chem. Mater.* **2001,** *13*, 308–311.
11. Peng, C. Y.; Zhang, H. J.; Yu, J. B.; Meng, Q. G.; Fu, L. S.; Li, H. R.; Sun, L. N.; Guo, X. N. Synthesis, Characterization, and Luminescence Properties of the Ternary Europium Complex Covalently Bonded to Mesoporous SBA-15. *J. Phys. Chem. B* **2005,** *109*, 15278–15287.
12. Li, D. M.; Zhang, J. L.; Anpo, M. Preparation of Organic−Inorganic Material from MCM-48 and Pyrylium Salt. *Opt. Mater.* **2005,** *27*, 671–673.
13. Wang, L. Z.; Liu, Y. L.; Chen, F.; Zhang, J. L.; Anpo, M. Manipulating Energy Transfer Processes between Rhodamine 6G and Rhodamine B in Different Mesoporous Hosts. *J. Phys. Chem. C* **2007,** *111*, 5541–5548.
14. Wang, L. Z.; Shao, Y. F.; Zhang, J. L.; Anpo, M. Study on the Fluorescence Properties of Fluorescein Dye Incorporated into SBA-15. *Opt. Mater.* **2006,** *28*, 1232–1234.
15. Shao, Y. F.; Wang, L. Z.; Zhang, J. L.; Anpo, M. The Photoluminescence of Rhodamine B Encapsulated in Mesoporous Si-MCM-48, Ce-MCM-48, Fe-MCM-48, and Cr-MCM-48 Molecular Sieves. *J. Photochem. Photobiol., A* **2006,** *180*, 59–64.
16. Zhao, W. J.; Li, D. M.; Bin, H.; Zhang, J. L.; Huang, J. Z.; Zhang, L. Z. The Photoluminescence of Coumarin Derivative Encapsulated in MCM-41 and Ti-MCM-41. *Dyes Pigm.* **2005,** *64*, 265–270.
17. Li, D. M.; Zhang, J. L.; Anpo, M. Study on the Fluorescence Properties of Benzopyrylium salt in Ti-HMS. *Dyes Pigm.* **2004,** *63*, 71–76.
18. Yang, P.; Quan, Z.; Lu, L.; Huang, S.; Lin, J. Luminescence Functionalization of Mesoporous Silica with Different Morphologies and Applications as Drug Delivery Systems. *Biomaterials* **2008,** *29*, 692–702.
19. Lai, C. Y.; Trewyn, B. G.; Jeftinija, D. M.; Jeftinija, K.; Xu, S.; Jeftinija, S.; Lin, V. S. Y. A Mesoporous Silica Nanosphere-Based Carrier System with Chemically Removable CdS Nanoparticle Caps for Stimuli-Responsive Controlled Release of Neurotransmitters and Drug Molecules. *J. Am. Chem. Soc.* **2003,** *125*, 4451–4459.
20. Liong, M.; Lu, J.; Kovochich, M.; Xia, T.; Ruehm, S. G.; Nel, A. E.; Tamanoi, F.; Zink, J. I. Multifunctional Inorganic Nanoparticles for Imaging, Targeting, and Drug Delivery. *ACS Nano* **2008,** *2*, 889–896.
21. Wang, L. Z.; Lei, J. Y.; Zhang, J. L. Building of Multifluorescent Mesoporous Silica Nanoparticles. *Chem. Commun.* **2009,** *16*, 2195–2197.
22. Ow, H.; Larson, D.; Srivastava, M.; Baird, B.; Webb, W.; Wiesner, U. Bright and Stable Core-Shell Fluorescent Silica Nanoparticles. *Nano Lett.* **2005,** *5*, 113–117.
23. Burns, A.; Ow, H.; Wiesner, U. Fluorescent Core-Shell Silica Nanoparticles: Towards 'Lab on a Particle' Architectures for Nanobiotechnology. *Chem. Soc. Rev.* **2006,** *35*, 1028–1042.
24. Choi, J.; Burns, A.; Williams, R.; Zhou, Z.; Flesken-Nikitin, A.; Zipfel, W.; Wiesner, U.; Niktin, A. Core-Shell Silica Nanoparticles as Fluorescent Labels for Nanomedicine *J. Biomed. Opt.* **2007,** *12*, 064007–064017.
25. Larson, D. R.; Ow, H.; Vishwasrao, H. D.; Heikal, A. A.; Wiesner, U.; Webb, W. W. Silica Nanoparticle Architecture Determines Radiative Properties of Encapsulated Fluorophores. *Chem. Mater.* **2008,** *20*, 2677–2684.
26. Herz, E.; Burns, A.; Bonner, D.; Wiesner, U. Large Stokes-Shift Fluorescent Silica Nanoparticles with Enhanced Emission Over Free Dye for Single Excitation Multiplexing. *Macromol. Rapid Commun.* **2009,** *30*, 1907–1910.
27. Burns, A.; Vider, J.; Ow, H.; Herz, E.; Penate-Medina, O.; Baumgart, M.; Larson, S. M.; Wiesner, U.; Bradbury, M. Fluorescent Silica Nanoparticles with Efficient Urinary Excretion for Nanomedicine. *Nano Lett.* **2009,** *9*, 442–448.
28. Herz, E.; Marchincin, T.; Connelly1, L.; Bonner, D.; Burns, A.; Switalsk, S.; Wiesner, U. Relative Quantum Yield Measurements of Coumarin Encapsulated in Core-Shell Silica Nanoparticles. *J. Fluoresc.* **2010,** *20*, 67–72.

29. Zhao, X.; Bagwe, R. P.; Tan, W. Development of Organic-Dye-Doped Silica Nanoparticles in a Reverse Microemulsion. *Adv. Mater.* **2004,** *16*, 173–176.
30. Pauwels, B.; Tendeloo, G. V.; Thoelen, C.; Rhijn, W. V.; Jacobs, P. A. Structure Determination of Spherical MCM-41 Particles. *Adv. Mater.* **2001,** *13*, 1317.
31. Lakowicz, J. R. *Principles of Fluorescence Spectroscopy*, 2nd ed.; Kluwer Academic: New York, 1999.
32. Förster, T. Transfer Mechanisms of Electronic Excitation. *Discuss. Faraday Soc.* **1959,** *27*, 7–17.
33. Li, M.; Reddy, R. G.; Bennett, R.; Silva, N. D.; Jones, L. R.; Thomas, D. D. A Fluorescence Energy Transfer Method for Analyzing Protein Oligomeric Structure: Application to Phospholamban. *Biophys. J.* **1999,** *76*, 2587–2599.
34. Minoofar, P. N.; Dunn, B. S.; Zink, J. I. Multiply Doped Nanostructured Silicate Sol-Gel Thin Films: Spatial Segregation of Dopants, Energy Transfer, and Distance Measurements. *J. Am. Chem. Soc.* **2005,** *127*, 2656–2665.
35. Selvin, P. R. Fluorescence Resonance Energy Transfer. *Methods Enzymol.* **1995,** *246*, 300–334.
36. Selvin, P. R. Lanthanide-Based Resonance Energy Transfer. *IEEE J. Sel. Top. Quantum Electron.* **1996,** *2*, 1077–1087.
37. Root, D. D.; Stewart, S.; Xu, J. Dynamic Docking of Myosin and Actin Observed with Resonance Energy Transfer. *Biochemistry* **2002,** *41*, 1786–1794.
38. Spagnuolo, C. C.; Vermeij, R. J.; Jares-Erijman, E. A. Improved Photostable FRET-Competent Biarsenical-Tetracysteine Probes Based on Fluorinated Fluoresceins. *J. Am. Chem. Soc.* **2006,** *128*, 12040–12041.
39. Patel, D. A.; Root, D. D. Close Proximity of Myosin Loop 3 to Troponin Determined by Triangulation of Resonance Energy Transfer Distance Measurements. *Biochemistry* **2009,** *48*, 357–369.
40. Xiao, M.; Selvin, P. R. Quantum Yields of Luminescent Lanthanide Chelates and Far-Red Dyes Measured by Resonance Energy Transfer. *J. Am. Chem. Soc.* **2001,** *123*, 7067–7073.
41. Delgadillo, R. F; Parkhurst, L. Spectroscopic Properties of Fluorescein and Rhodamine Dyes Attached to DNA *J. Photochem. Photobiol.* **2010,** *86*, 261–272.
42. Förster, T. Delocalized Excitation and Excitation Transfer. In *Modern Quantum Chemistry; Istanbul Lectures*, Part III; Sinanoglu, O., Ed.; Academic: New York, 1965; p 93.